

## Supporting Information

### Orientation selection in high-field RIDME and PELDOR experiments involving low-spin Co<sup>II</sup> ions

*Angeliki Giannoulis,<sup>a,b</sup> Claire L. Motion,<sup>c</sup> Maria Oranges,<sup>a,b</sup> Michael Bühl,<sup>a</sup> Graham M. Smith<sup>c</sup> and Bela E.*

*Bode<sup>\*,a,b</sup>*

<sup>a</sup>EaStCHEM School of Chemistry and Centre of Magnetic Resonance, University of St Andrews, North Haugh, St Andrews, Fife, KY16 9ST, UK

<sup>b</sup>Biomedical Sciences Research Complex, University of St Andrews, North Haugh, St Andrews, Fife, KY16 9ST, UK

<sup>c</sup>SUPA, School of Physics & Astronomy, University of St Andrews, North Haugh, St Andrews, Fife, KY16 9SS, UK

## **Table of Contents**

EPR sample preparation	S3
EPR instrumentation and data collection	S3
Data analysis	S3
Experimental parameters	S4
Theoretical background	S5
Details on results	S5
Field sweep spectra	S6
Measurements of longitudinal relaxation	S7
Primary data and analysis	S7
DFT calculation details	S21
References	S22

## EPR sample preparation

The synthesis of the spin-labelled terpyridine ligand **L** was performed as described previously.<sup>1, 2</sup> CoCl<sub>2</sub>, anhydrous ≥98%, DMSO-*d*<sub>6</sub> and D<sub>2</sub>O were obtained from Sigma-Aldrich, EtOH from VWR and CH<sub>2</sub>Cl<sub>2</sub> and ethylene glycol from Fischer Scientific. For EPR measurements **1** was prepared *in situ* by adding a CoCl<sub>2</sub> solution in EtOH (25 μL, 200 μM) to a solution of **L** in CH<sub>2</sub>Cl<sub>2</sub> (50 μL, 200 μM) and mixing for 30 s. The solvents were evaporated *in vacuo*, the residue was re-dissolved in 75 μL DMSO-*d*<sub>6</sub>/D<sub>2</sub>O/ethylene glycol (8/1/1). NaBPh<sub>4</sub> was added (10-fold excess) to enhance solubility and to improve glass formation upon freezing. The solution was transferred to a 3 mm OD FEP sample tube (Adtech) for W-band measurements and to a 3 mm quartz EPR tube (Wilmad) for Q-band measurements before being flash frozen by rapid immersion into liquid nitrogen.

## EPR instrumentation and data collection

Co-NO distance measurements were performed with the five-pulse RIDME<sup>3, 4</sup> ( $\pi/2 - \tau_1 - \pi - (\tau_1+t) - \pi/2 - T_{\text{mix}} - \pi/2 - (\tau_2-t) - \pi - \tau_2 - \text{echo}$ ) and four-pulse PELDOR<sup>5-7</sup> ( $\pi/2(f_{\text{obs}}) - \tau_1 - \pi(f_{\text{obs}}) - (\tau_1+t) - \pi(f_{\text{pump}}) - (\tau_2-t) - \pi(f_{\text{obs}}) - \tau_2 - \text{echo}$ ) pulse sequences and NO-NO distance measurements using four-pulse PELDOR. No phase cycling and an 8-step phase cycling was applied for PELDOR and RIDME measurements, respectively. Longitudinal relaxation of the cobalt was measured with inversion recovery sequence ( $\pi - T - \pi/2 - \tau - \pi - \tau - \text{echo}$ ). Measurements were recorded either at W-band frequencies (~94.0 GHz) on a home-built high power pulsed spectrometer (HiPER)<sup>8, 9</sup> incorporating a continuous flow helium cryostat (CF935) and a temperature control system (ITC 502) from Oxford Instruments or at Q-band frequencies (~34.0 GHz) using a Bruker Elexsys E580 pulsed EPR spectrometer including the second frequency option (E580-400U). At Q-band pulses were amplified by travelling wave tube (TWT) amplifier (150 W) from Applied Systems Engineering and a TE012 cavity with flex line probe head was used. The sample temperature was stabilized with a cryogen-free variable temperature cryostat (Cryogenic Ltd). PELDOR measurements varied between 12 min to 1h and RIDME measurements were all run for 20 min.

## Data analysis

**RIDME and PELDOR measurements.** RIDME background correction was performed by fitting a second order polynomial function while PELDOR background correction was performed by fitting a background homogeneous in three dimensions leading to a reasonable fit and dipolar spectrum judged by visual inspection. The data was inverted to distance distributions using Tikhonov Regularization<sup>10</sup> in DeerAnalysis2013.<sup>11</sup> The regularization parameter used for all data was 1. Distance distributions by Tikhonov Regularization are shown for illustrative purposes and demonstrated how orientation selection leads to poor fits of the dipolar spectra or even distance peaks shifted by  $1/2^{1/3} \sim 0.79$  corresponding to  $\theta=0^\circ$ . For the nitroxide-nitroxide PELDOR the limited dipolar evolution time might reduce the reliability of the distance distributions. Thus, validations of the obtained distributions were performed by varying the background start range from 5% to 80% of the primary time window in 16 trials and only data sets exceeding the lowest root mean square deviation by a maximum of 15% (prune level) were used. All modulation depth values are given in Table S6.

**Inversion recovery (IR) measurements.** The IR data were phase-corrected and normalized.

## Experimental parameters

**Table S1.** Parameters of the field sweep Co and NO spectra at W- and Q-band frequencies.

	Co W-band	NO W-band	Co Q-band	NO Q-band
Temperature [K]	11	30	30	30
$\pi/2$ pulse length [ns]	5	6.5	16	16
$\pi$ pulse length [ns]	10	13	32	32
$\tau$ [ns]	250	400	160	160

**Table S2.** Parameters of the W-band Co-NO and NO-NO PELDOR measurements.

	Co-NO			NO-NO					
	NOx	NOy	NOz	xx	yy	zz	xy	zy	zx
Temperature [K]	15	15	15	10	10	10	10	10	10
$\pi/2$ pulse length [ns]	6	6	6	6	16	12	6	16	6
$\pi$ pulse length [ns]	12	12	12	12	32	24	12	32	12
Pump pulse length [ns]	12	13	12	13	28	26	10	38	18
$\tau_1$ [ns]	250	250	250	200	200	200	200	200	200
$\tau_2$ [ $\mu$ s]	850	850	850	4.8	4.8	4.8	4.8	4.8	4.8
starting $t$ [ns]	-100	-100	-100	-100	-100	-100	-100	-100	-100
$\Delta t$ [ns]	8	8	8	20	20	20	20	20	20
repetition rate [ms]	1	1	1	50	50	50	50	50	50

**Table S3.** Parameters of the W- and Q-band Co-NO RIDME measurements.

	W-band	Q-band
Temperature [K]	30	30
$\pi/2$ pulse length [ns]	24	16
$\pi$ pulse length [ns]	48	32
$\tau_1$ [ns]	400	400
$\tau_2$ [ $\mu$ s]	2.4	2.0
$T_{\text{mix}}$ [ $\mu$ s]	25	50
starting $t$ [ns]	-200	-200
$\Delta t$ [ns]	8	8
repetition rate [ms]	10	10

**Table S4.** Parameters of the inversion recovery measurements on the Co ion at W- and Q-band frequencies.

	W-band	Q-band
Temperature [K]	30	30
$\pi/2$ pulse length [ns]	9	16
$\pi$ pulse length [ns]	18	32
$\tau$ [ns]	250	800
starting $T$ [ns]	-*	-500
$\Delta T$ [ns]	100	1000
repetition rate [ms]	1	0.6

\*the experiment was single run without phase cycling thus no starting value applied

## Theoretical background

### *Nitroxide principal axes*

The principal axes of the nitroxide, is defined as follows:  $g_x$  is co-linear to the N-O bond,  $g_y$  orthogonal to the  $g_x$  axis and in the plane formed between the nitroxyl group and its  $\alpha$ -substituents and  $g_z$  is perpendicular to both  $g_x$ ,  $g_y$  (see Figure 1, A).

### *Structural model and predicted results*

#### Structural model

Given the symmetry of the NO tensors in **1** (Figure 1, A) it is expected the  $x$ -direction of NO to be parallel to  $r_{\text{NO-NO}}$  while  $y$ ,  $z$ -directions to be perpendicular. Deviations from this simple case are expected to arise due to small structural flexibility of the complex and due to rotation of the ester bond creating a cone of angles of  $25^\circ$ – $30^\circ$ <sup>12, 13</sup> along the backbone causing admixture of  $y$  and  $z$  directions.

#### Predicted results in the Co-NO RIDME experiment

The Co-NO RIDME experiment is expected to yield information on the relative orientation of  $r_{\text{Co-NO}}$  with the nitroxide axes and is expected to be in line with the assignment of the  $r_{\text{NO-NO}}$  with respect to the nitroxide axes from NO-NO PELDOR measurements. The experiment is not expected to yield any information on the Co  $g$ -tensor since the spin flip of the Co ion is induced due to spontaneous longitudinal relaxation.

#### Predicted results in the NO-NO PELDOR experiment

The Co-NO PELDOR experiment is expected to yield the double frequency for the  $xx$  measurement since the  $x$  axes of the two nitroxides in the ligands are collinear. All combinations of  $x$  with  $y$  or  $z$  components should yield no or little (due to deviations from linearity and ester bond rotation) modulation since these combinations are orthogonal or almost orthogonal to each other. Finally, all  $y$ ,  $z$  combinations should have  $r_{\text{NO-NO}}$  perpendicular to the magnetic field yielding the single frequency in the PELDOR experiment.

#### Predicted results in the Co-NO PELDOR experiment

The Co-NO PELDOR experiment where only the low cobalt  $g$ -value can be observed with our W-band spectrometer would be expected to select Co  $g_z$ . Considering both the  $g_z$  tensor of Co and the  $g_x$  tensor of NO to be oriented parallel to  $r_{\text{Co-NO}}$  it would be anticipated that the Co-NO  $g_x$  PELDOR measurement would yield the double frequency  $\nu_{\parallel}$ , while Co-NO PELDOR measurements inverting  $y$ - or  $z$ - directions of the nitroxide would yield little or no modulation as they are not collinear to the  $r_{\text{Co-NO}}$ .

## Details on results

### NO-NO PELDOR experiments

Due to the symmetry of pairs, NO-NO OS-PELDOR was performed at six detection/inversion positions of NO and at W-band where NO  $g$ -anisotropy is well resolved.

Experiments on  $xx$  should yield  $\nu_{\parallel}$ , all combinations of  $y$ ,  $z$  directions (*i.e.*  $yy$ ,  $yz$ ,  $zz$ ,  $zy$ ) should give  $\nu_{\perp}$ , while no modulation is expected for measurements pairing  $x$  with  $y$  or  $z$  (*i.e.*  $xz$ ,  $zx$ ,  $yx$ ,  $xy$ ) as these two orientations will not coincide within a single complex irrespective of its overall orientation (Table S5, top).

Performing the experiment at  $xx$ ,  $xy$  mainly  $\nu_{\parallel}$  is observed, *i.e.* molecules with  $r_{\text{NO-NO}}$  parallel to the magnetic field. The surprisingly large modulation depth of the  $xy$  measurement (approximated to zero in the initial prediction) can be explained given that the highest intensity part of the NO spectrum is inverted and assuming tilting of the nitroxide  $y$ -axis towards the  $r_{\text{NO-NO}}$  distance vector that has the latter lie between the NO  $g_x$  and  $g_y$  axes, as well as a non-perfectly collinear geometry of the NO  $x$ -axis with the  $r_{\text{NO-NO}}$ . Nevertheless, the results are in excellent agreement with previously reported W-band data on shorter and covalently linked rigid bis-nitroxides where these deviations had been simulated to be accounted for the ester bond rotation in an  $25^\circ$  cone angle.<sup>12, 13</sup> The experiment on  $xx$  features the largest modulation depth as would be expected due to both detecting and inverting spins at  $x$  and is in accordance with the model.

Measurements at  $zz$ , and  $zy$  yielded  $\nu_{\perp}$  in good agreement with our geometrical considerations. The  $zx$  measurement features the shallowest modulation depth in line with our prediction that observing  $g_x$  of one NO while inverting  $g_z$  the other NO should not yield dipolar modulation as there will be no dipolar angle that has both orientations present.

The low modulation depth of  $zz$  measurement can be explained considering the low spectral intensity on the  $g_z$  edge of the spectrum.

The W-band OS-NO-NO PELDOR data on **1** confirm our coarse initial model reasonably well and are in excellent agreement with a structurally very similar but shorter covalent bis-nitroxides.<sup>12, 13</sup> Additionally, the data confirm the rigidity of the bis-terpyridine motif that links the two nitroxides.

**Table S5.** Expected (top) and experimentally observed (bottom) dipolar frequencies of the NO-NO PELDOR with modulation depth values in parentheses. Grey font color corresponds to deviations from the model, while ‘DNR’ means these measurements were not run.

	$x$	$y$	$z$
$x$	$\nu_{\parallel}$	-	-
$y$	-	$\nu_{\perp}$	$\nu_{\perp}$
$z$	-	$\nu_{\perp}$	$\nu_{\perp}$

	$x$	$y$	$z$
$x$	$\nu_{\parallel}$ (0.244)	DNR	DNR
$y$	$\nu_{\parallel}$ (0.215)	$\nu_{\perp}$ (0.100)	DNR
$z$	$\nu_{\perp}$ (0.058)	$\nu_{\perp}$ (0.124)	$\nu_{\perp}$

## Field sweep spectra

The field swept spectra of cobalt and nitroxide at W- and at Q-band are shown in Figure S1.

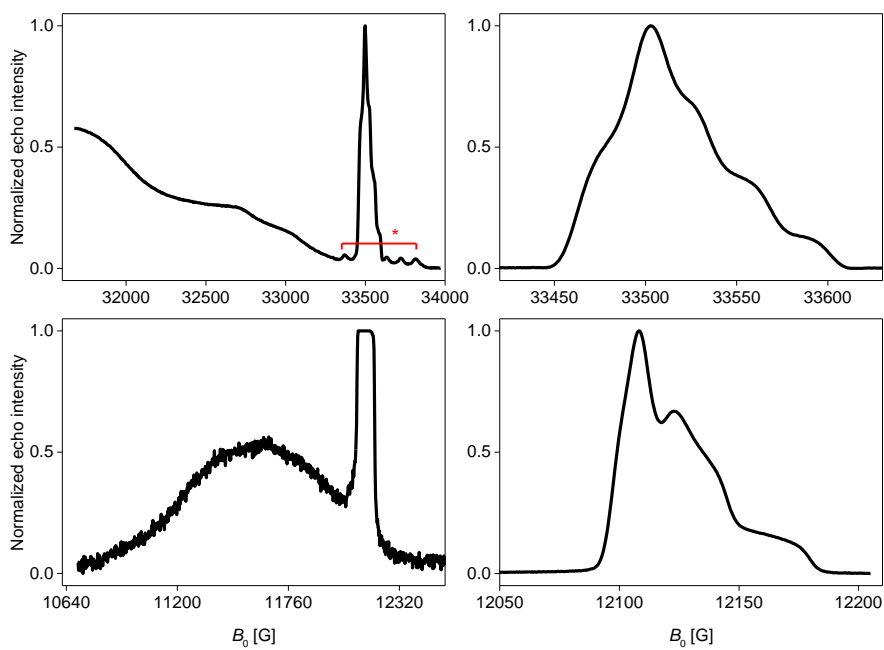


**Figure S1.** Field swept spectra of the cobalt and of the nitroxide at W- (top left and right, respectively) and Q-band (bottom left and right, respectively). The five peaks marked with asterisk at the W-band spectrum of Co are due to the presence of manganese ( $S=5/2$ ) impurity.

The cobalt ion exhibits a broad EPR spectrum (more than 1650 G at W-band and 1260 G at Q-band) at lower magnetic fields with respect to the nitroxide. Due to bandwidth limitations of the W-band spectrometer only a part of the cobalt's spectrum could be recorded, *i.e.* the low  $g$ -component close to the nitroxide. The five peaks marked with asterisk at the W-band spectrum are due to the presence of manganese ( $S=5/2$ ) impurity either from the FEP sample tube or the sample itself, which is only observed below  $\sim 15$  K. The nitroxide  $g$ -anisotropy spreads over 160 G at W-band and over 100 G at Q-band. Thus, we expect orientation selective measurements for both spin centers to be better resolved at the high frequency band.

### Measurements of longitudinal relaxation

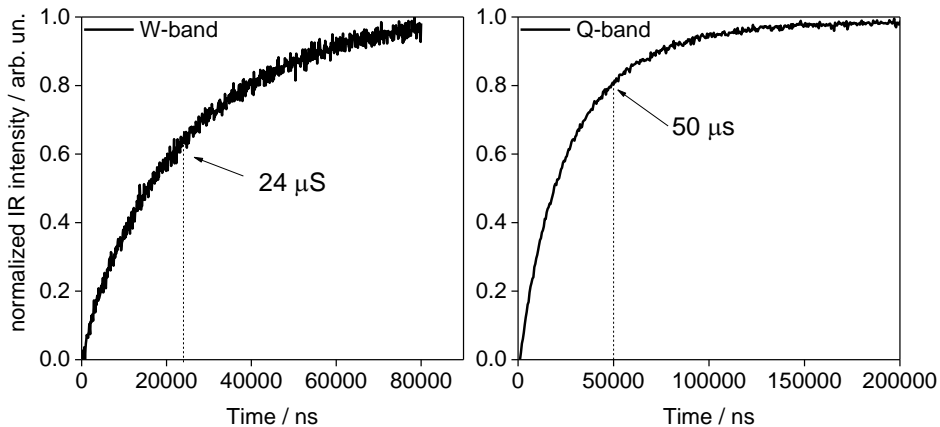


**Figure S2.** Longitudinal relaxation of cobalt ion at W- (left) and Q-band (right) measured with inversion recovery sequence.

In order to estimate the mixing time ( $T_{\text{mix}}$ ) of the RIDME experiments we measured longitudinal relaxation rates of the Co ion at 30 K. The  $T_{\text{mix}}$  values used at W- and Q-band are indicated with arrows.

### Primary data and analysis

The primary and background-free RIDME and PELDOR data, along with their Fourier transform spectra and distance distributions are given in Figures S3-S25.

## W-band Co-NO PELDOR

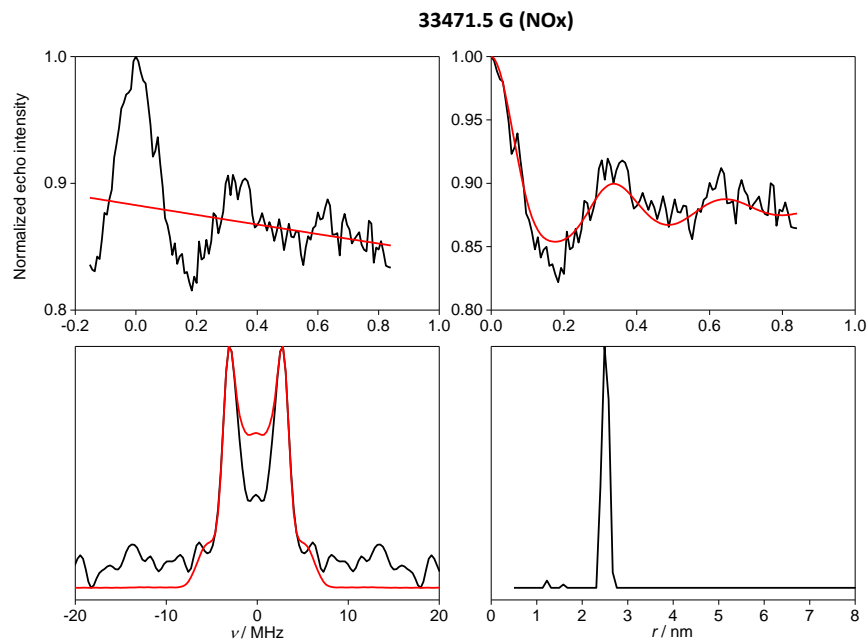


**Figure S3.** Primary (top left) and background corrected (top right) PELDOR time traces and corresponding frequency spectrum (bottom left) and distance distribution (bottom right) for the Co-NO distance measurement at W-band inverting NO at 33471.5 G (NO<sub>x</sub>).

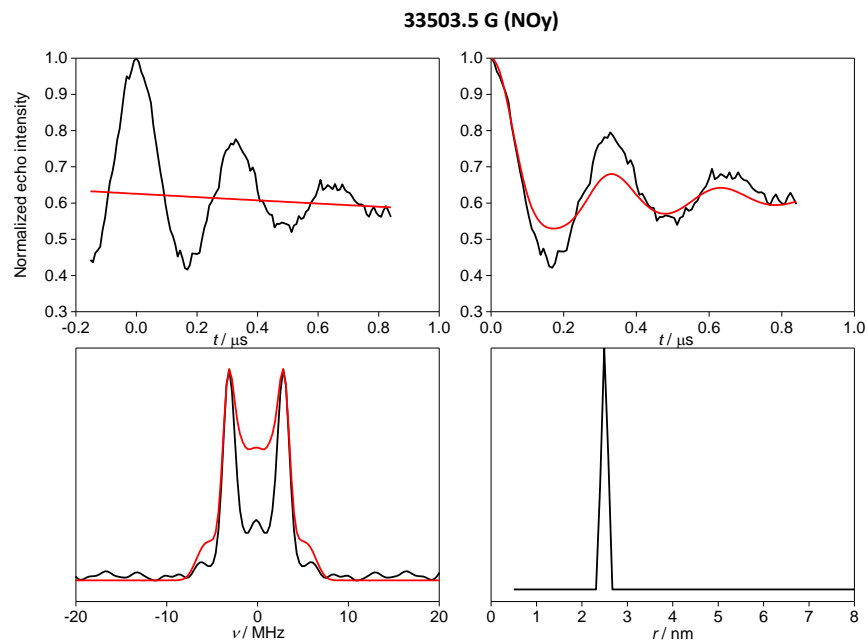


**Figure S4.** Primary (top left) and background corrected (top right) PELDOR time traces and corresponding frequency spectrum (bottom left) and distance distribution (bottom right) for the Co-NO distance measurement at W-band inverting NO at 33503.5 G (NO<sub>y</sub>).

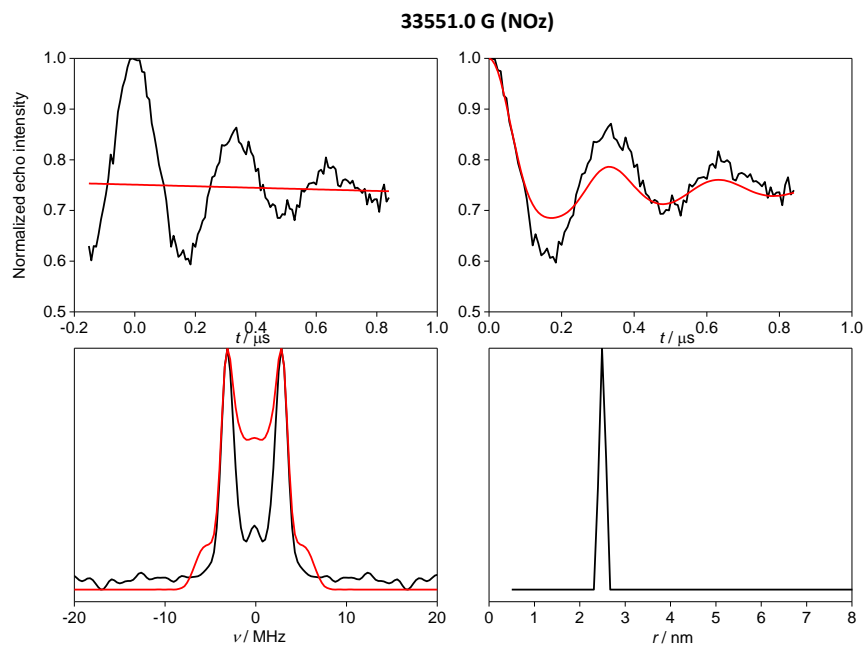


**Figure S5.** Primary (top left) and background corrected (top right) PELDOR time traces and corresponding frequency spectrum (bottom left) and distance distribution (bottom right) for the Co-NO distance measurement at W-band inverting NO at 33551.5 G (NOz).

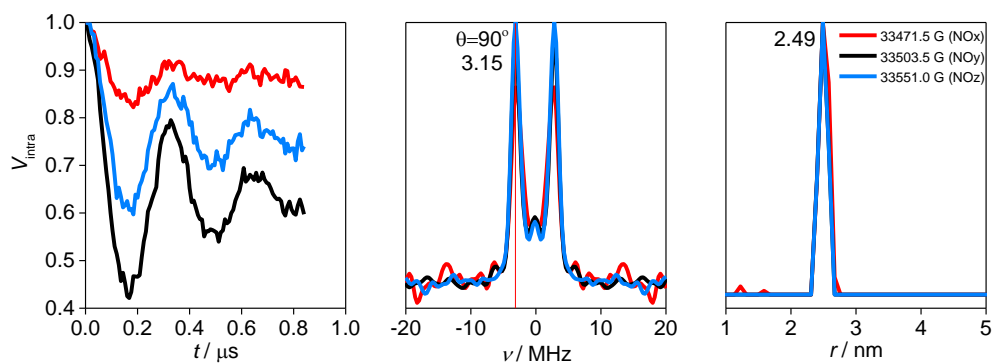


**Figure S6.** Comparison of W-band Co-NO PELDOR measurements. Background corrected PELDOR time traces (left), frequency spectra (middle) and distance distributions (right).

## W-band NO-NO PELDOR

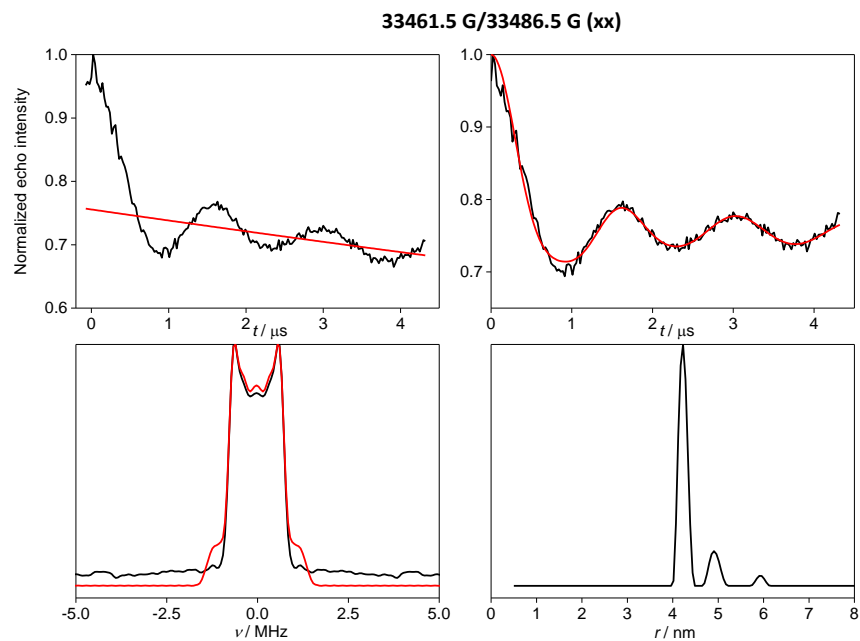


**Figure S7.** Primary (top left) and background corrected (top right) PELDOR time traces and corresponding frequency spectrum (bottom left) and distance distribution (bottom right) for the NO-NO distance measurement at W-band inverting NO at 33486.5 G (NO<sub>x</sub>) and observing NO at 33461.5 G (NO<sub>x</sub>).

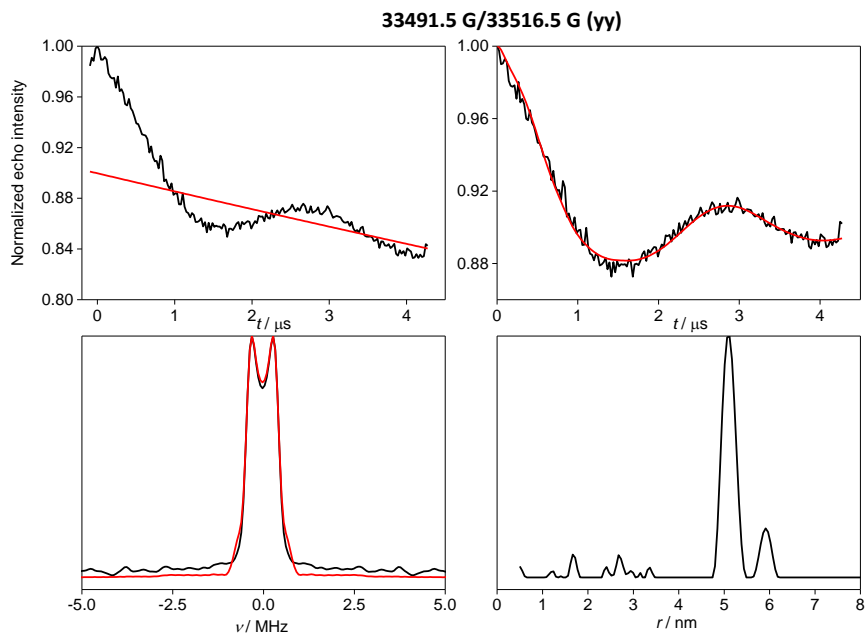


**Figure S8.** Primary (top left) and background corrected (top right) PELDOR time traces and corresponding frequency spectrum (bottom left) and distance distribution (bottom right) for the NO-NO distance measurement at W-band inverting NO at 33516.5 G (NO<sub>y</sub>) and observing NO at 33491.5 G (NO<sub>y</sub>).

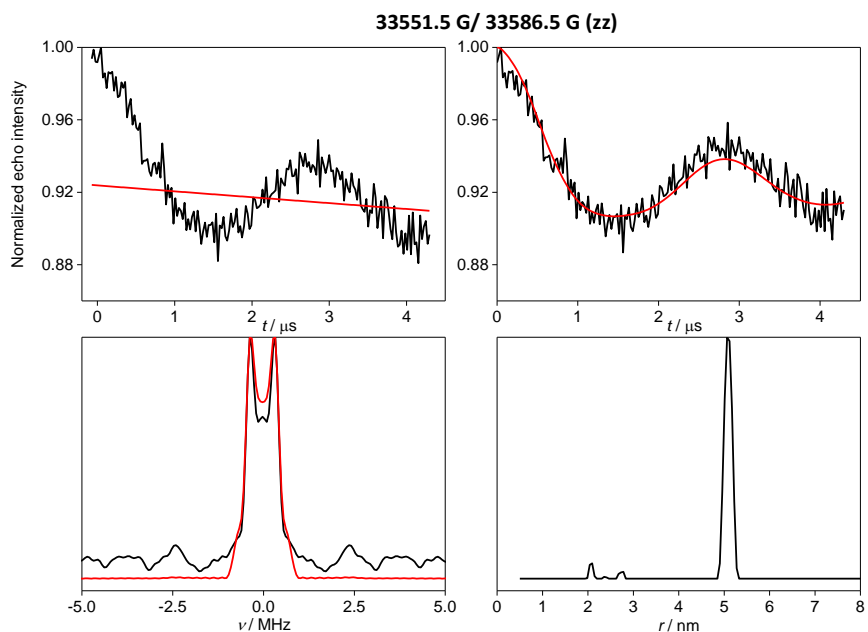


**Figure S9.** Primary (top left) and background corrected (top right) PELDOR time traces and corresponding frequency spectrum (bottom left) and distance distribution (bottom right) for the NO-NO distance measurement at W-band inverting NO at 33586.5 G (NOz) and observing NO at 33551.5 G (NOz).

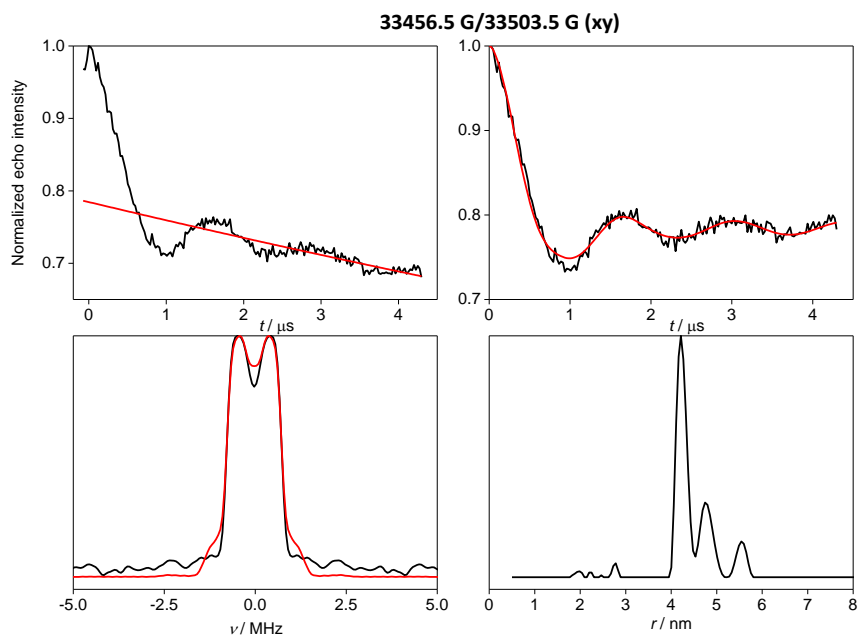


**Figure S10.** Primary (top left) and background corrected (top right) PELDOR time traces and corresponding frequency spectrum (bottom left) and distance distribution (bottom right) for the NO-NO distance measurement at W-band inverting NO at 33503.5 G (NOy) and observing NO at 33456.5 G (NOx).

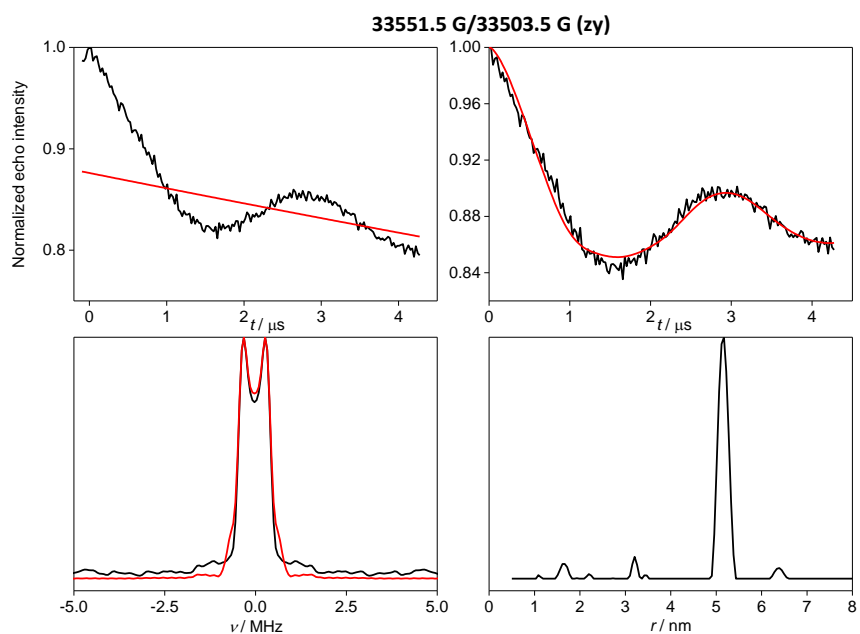


**Figure S11.** Primary (top left) and background corrected (top right) PELDOR time traces and corresponding frequency spectrum (bottom left) and distance distribution (bottom right) for the NO-NO distance measurement at W-band inverting NO at 33503.5 G (NO<sub>y</sub>) and observing NO at 33551.5 G (NO<sub>z</sub>).

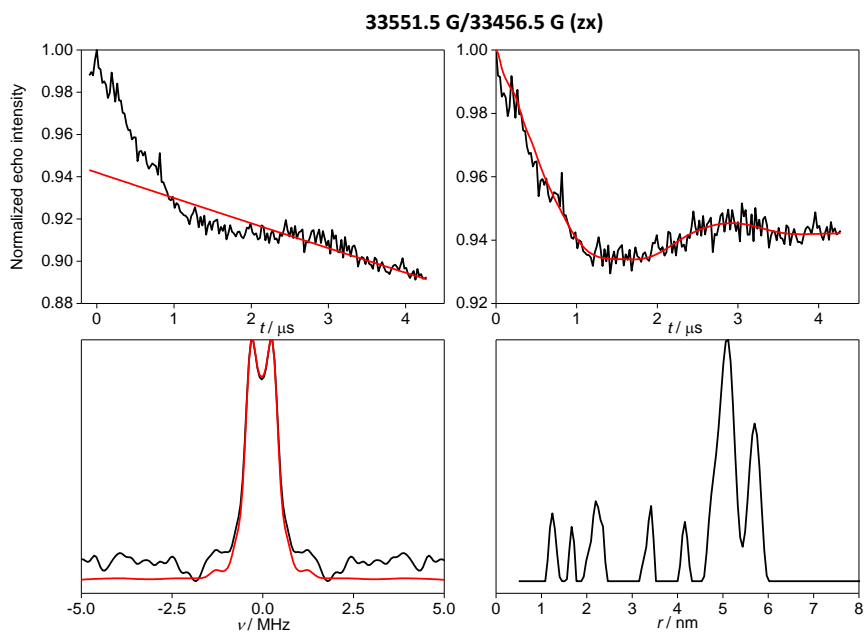


**Figure S12.** Primary (top left) and background corrected (top right) PELDOR time traces and corresponding frequency spectrum (bottom left) and distance distribution (bottom right) for the NO-NO distance measurement at W-band inverting NO at 33456.5 G (NO<sub>x</sub>) and observing NO at 33551.5 G (NO<sub>z</sub>).

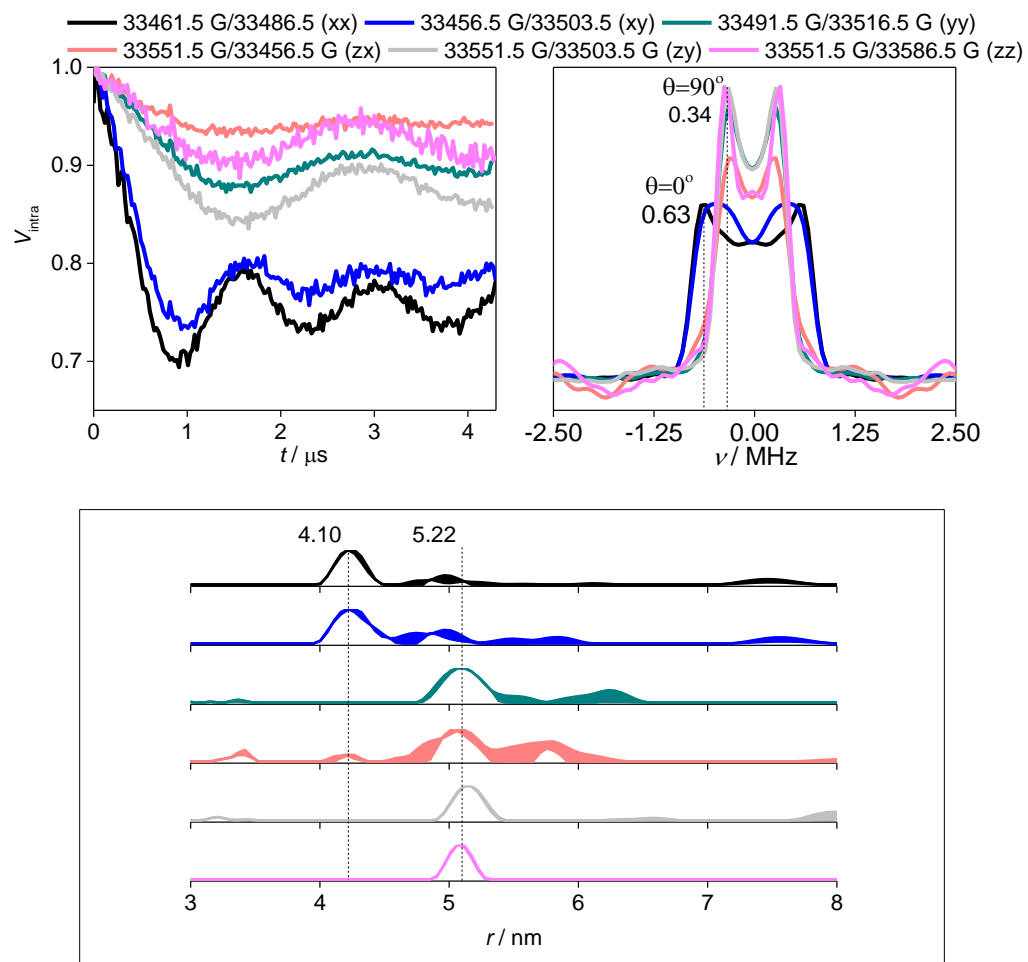


**Figure S13.** Comparison of W-band NO-NO PELDOR measurements. Background corrected PELDOR time traces (top left), frequency spectra (top right) and distance distributions after validation (bottom).

## W-band Co-NO RIDME

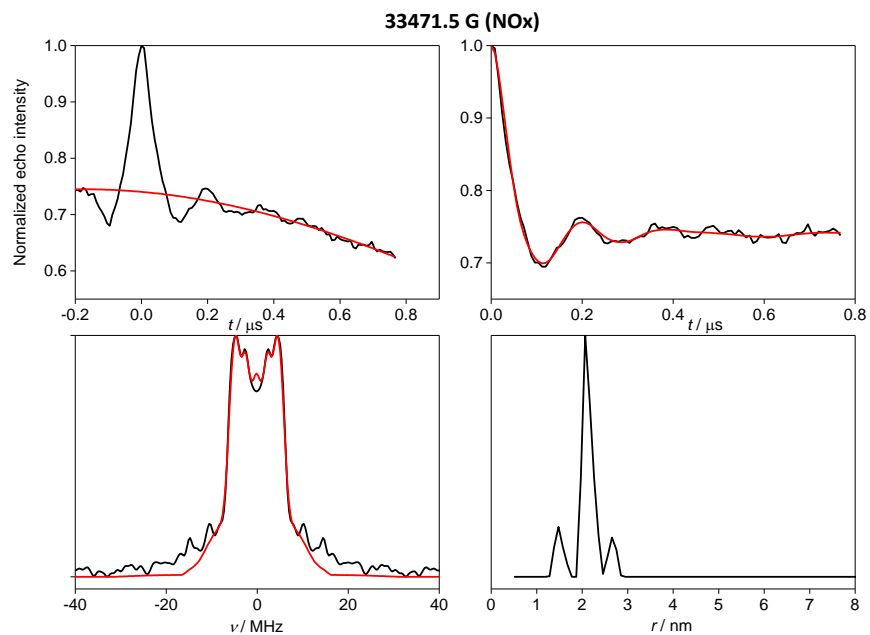


**Figure S14.** Primary (top left) and background corrected (top right) RIDME time traces and corresponding frequency spectrum (bottom left) and distance distribution (bottom right) for the Co-NO distance measurement at W-band observing NO at 33471.5 G (NO<sub>x</sub>).

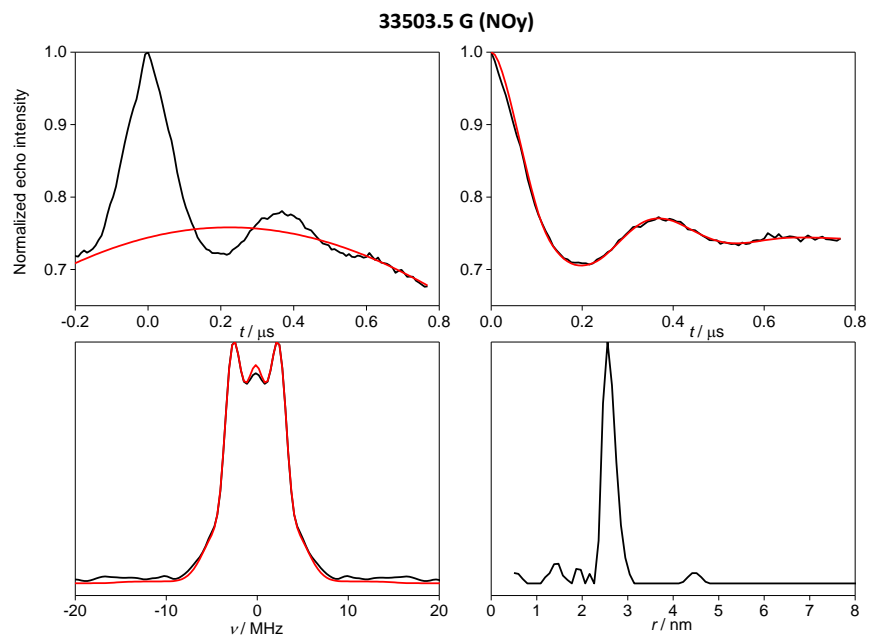


**Figure S15.** Primary (top left) and background corrected (top right) RIDME time traces and corresponding frequency spectrum (bottom left) and distance distribution (bottom right) for the Co-NO distance measurement at W-band observing NO at 33503.5 G (NO<sub>y</sub>).

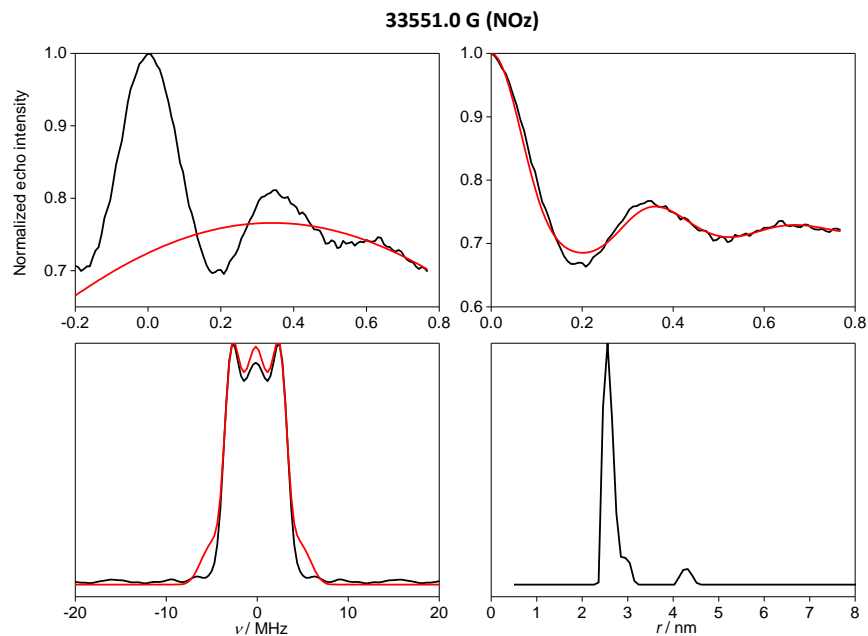


**Figure S16.** Primary (top left) and background corrected (top right) RIDME time traces and corresponding frequency spectrum (bottom left) and distance distribution (bottom right) for the Co-NO distance measurement at W-band observing NO at 33551.0 G (NOz).

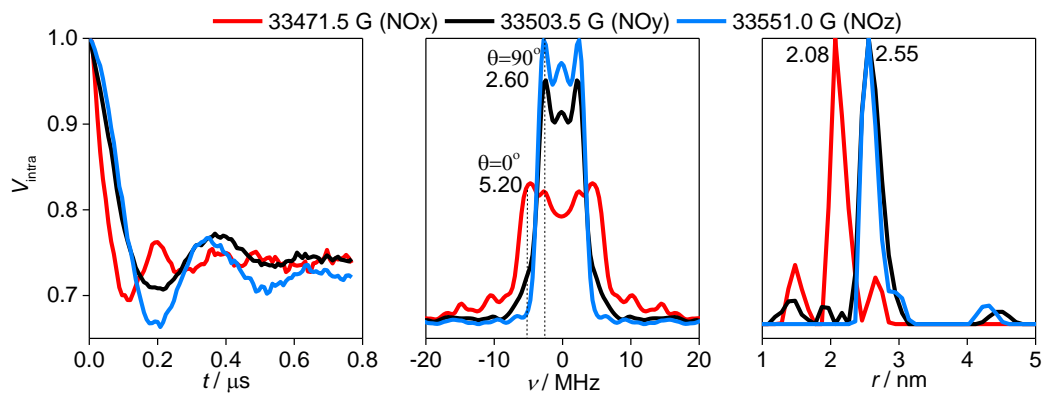


**Figure S17.** Comparison of W-band Co-NO RIDME measurements. Background corrected RIDME time traces (left), frequency spectra (middle) and distance distributions (right).

Figure S18 shows the effect of ESEEM to the W-band RIDME measurement observing NO using increasing  $\pi/2$ - $\pi$  pulse lengths.

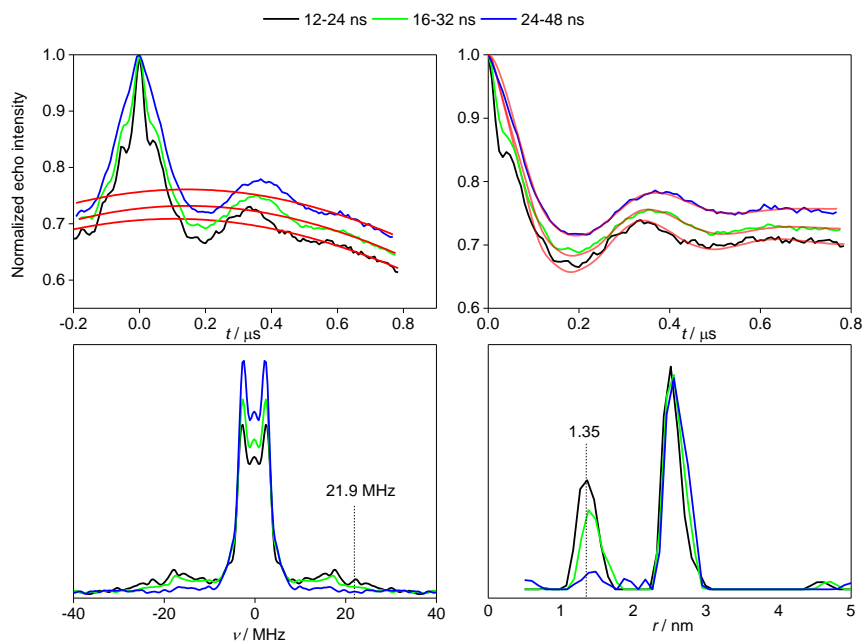


**Figure S18.** W-band Co-NO RIDME measurements observing NO at 33503.5 G with increasing pulse lengths. Primary (top left) and background corrected (top right) RIDME time traces and corresponding frequency spectrum (bottom left) and distance distribution (bottom right).

Observing NO at 33503.5 G with 12-24 ns pulses yielded the expected 2.6 nm Co-NO peak together with a shorter peak at 1.35 nm. In the frequency domain spectrum the 1.35 nm peak corresponds to the 21.9 MHz signal, in good accordance with the expected  $^2\text{H}$  Larmor frequency of 21.2 MHz at 33503.5 G. Increase of the pulse lengths to 24-48 ns almost eliminated ESSEM due to the smaller excitation bandwidth of these pulses with respect to the less selective 12-24 ns pulses.

## Q-band Co-NO RIDME

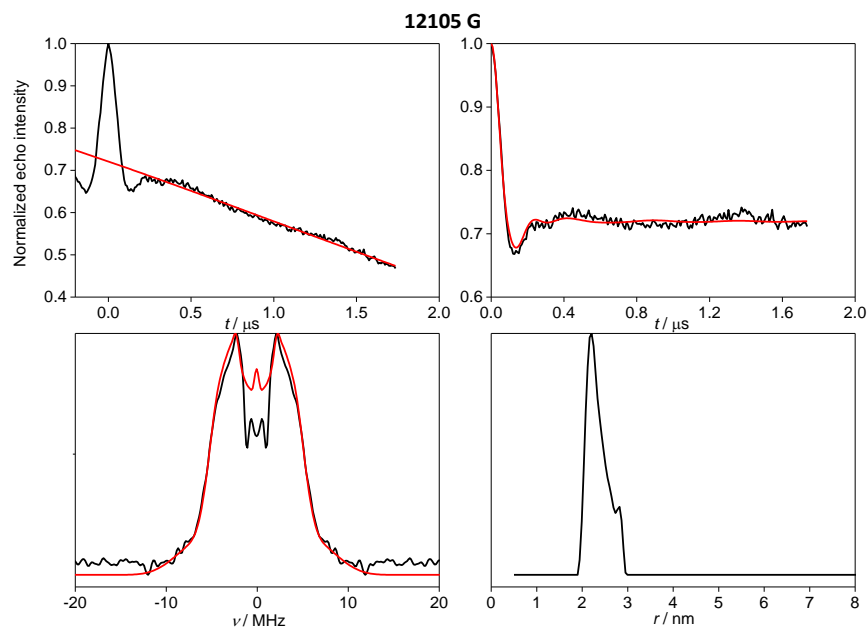


**Figure S19.** Primary (top left) and background corrected (top right) RIDME time traces and corresponding frequency spectrum (bottom left) and distance distribution (bottom right) for the Co-NO distance measurement at Q-band observing NO at 12105 G.

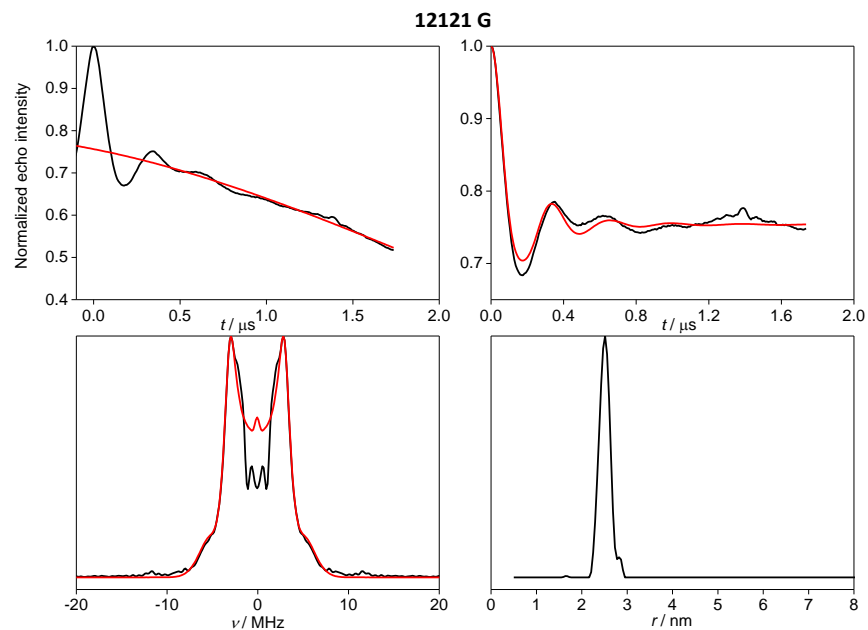


**Figure S20.** Primary (top left) and background corrected (top right) RIDME time traces and corresponding frequency spectrum (bottom left) and distance distribution (bottom right) for the Co-NO distance measurement at Q-band observing NO at 12121 G.

Measurement at 12154 G was performed with both 16-32 ns and 32-64 ns  $\pi/2$ - $\pi$  pulses. The longer pulses allowed resolving orientation selection better as would be anticipated due to their smaller excitation bandwidth with respect to the 16-32 ns pulses (Figures S21-S23).

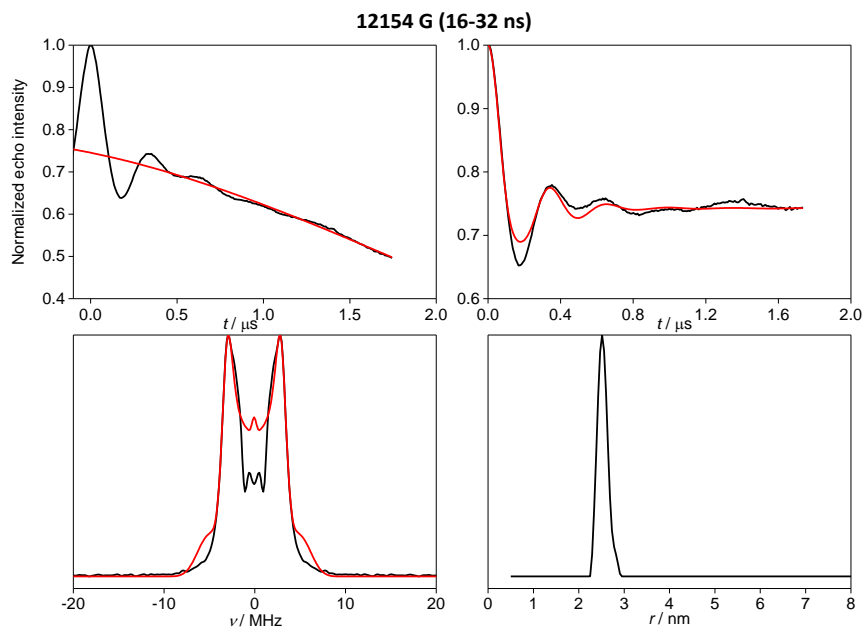


**Figure S21.** Primary (top left) and background corrected (top right) RIDME time traces and corresponding frequency spectrum (bottom left) and distance distribution (bottom right) for the Co-NO distance measurement at Q-band observing NO at 12154 G using 16-32 ns ( $\pi/2$ - $\pi$ ) pulses.

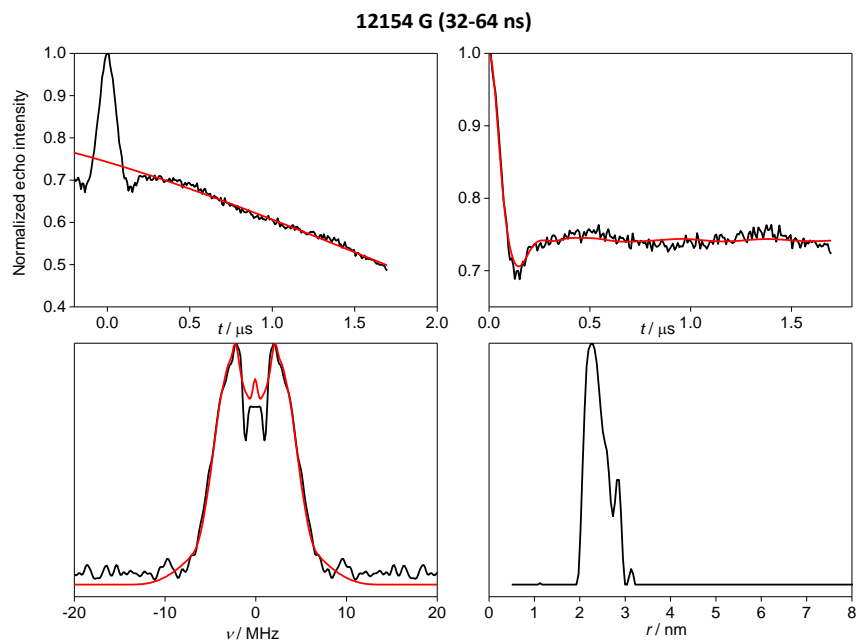


**Figure S22.** Primary (top left) and background corrected (top right) RIDME time traces and corresponding frequency spectrum (bottom left) and distance distribution (bottom right) for the Co-NO distance measurement at Q-band observing NO at 12154 G using 32-64 ns ( $\pi/2-\pi$ ) pulses.

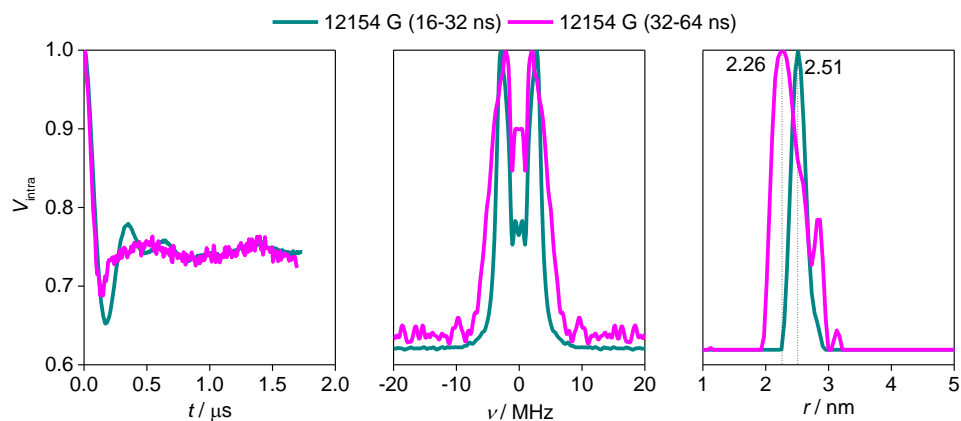


**Figure S23.** Comparison of Q-band Co-NO RIDME measurements observing nitroxide at 12154 G. Background corrected RIDME time traces (left), frequency spectra (middle) and distance distributions (right) measured with 16-32 (cyan) and 32-64 ns (magenta) pulses.

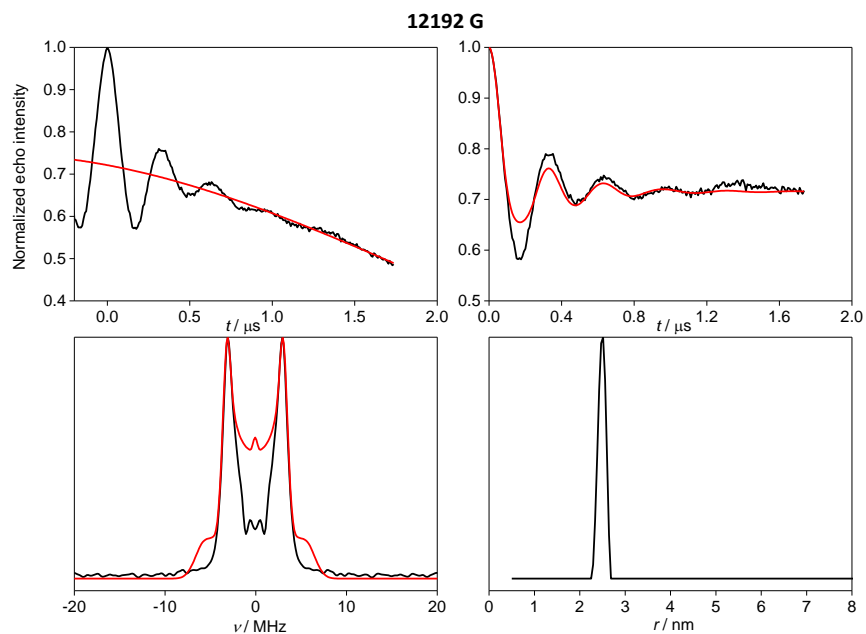


**Figure S24.** Primary (top left) and background corrected (top right) RIDME time traces and corresponding frequency spectrum (bottom left) and distance distribution (bottom right) for the Co-NO distance measurement at Q-band observing NO at 12192 G.

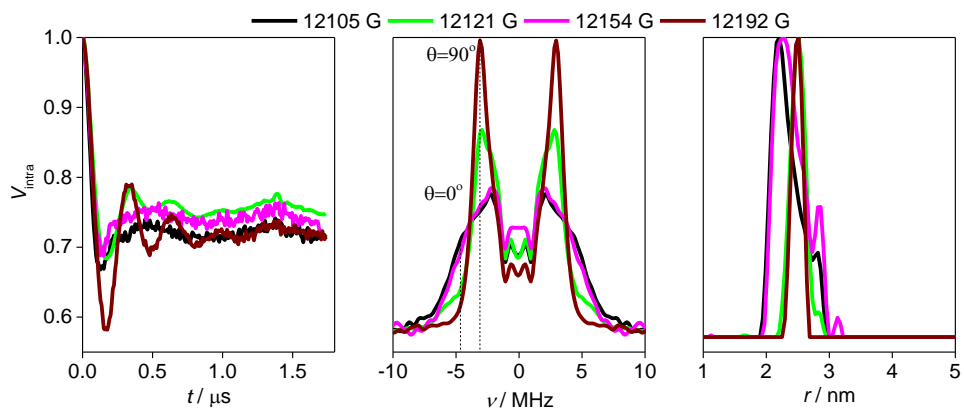


**Figure S25.** Comparison of Q-band Co-NO RIDME measurements. Background corrected RIDME time traces (left), frequency spectra (middle) and distance distributions (right).

**Table S6.** Modulation depth values for all distance measurements. $\Delta_{\text{NO-NO}}$  Q-band PELDOR (observe/pump)

$xx$	$xy$	$yy$	$zx$	$zy$	$zz$
0.244	0.215	0.100	0.058	0.124	0.076

 $\Delta_{\text{Co-NO}}$  W-band RIDME (observe NO  $g$ -tensor)

$x$	$y$ (12-24 ns)	$y$ (16-32 ns)	$y$ (24-48 ns)	$z$
0.260	0.239	0.273	0.244	0.276

 $\Delta_{\text{Co-NO}}$  Q-band RIDME (observe NO field (G))

12105	12121	12154 (16-32 ns)	12154 (32-64 ns)	12192
0.279	0.244	0.253	0.255	0.279

 $\Delta_{\text{Co-NO}}$  W-band PELDOR (invert NO  $g$ -tensor)

$x$	$y$	$z$
0.117	0.374	0.249

**DFT calculation details**

The structure of pristine  $[\text{Co}(\text{terpy})_2]^{2+}$  in its low-spin doublet state was optimised with the Gaussian 09 program<sup>14</sup> at the PBE0<sup>15-18</sup>-D3<sup>19-21</sup> level of density functional theory, imposing  $C_{2v}$  symmetry and employing AE1 basis,<sup>22, 23</sup> *i.e.*, a Wachters basis augmented with two diffuse  $p$  and one diffuse  $d$  sets for Co (8s7p4d, full contraction scheme 62111111/3311111/3111) and 6-31G\* for all other atoms. Spin contamination in the unrestricted Kohn-Sham wavefunction was negligible ( $\langle S^2 \rangle = 0.76$  instead of 0.75 expected for a doublet), and the minimum nature of this stationary point was confirmed by computation of the harmonic vibrational frequencies, which were all real. The pattern of the Co-N distances observed in the solid (two short nonequivalent distances to the "axial", *i.e.* central pyridine moieties and two pairs of longer distances to the "equatorial", *i.e.* terminal pyridines)<sup>24</sup> is well reproduced at that level. The  $g$  tensor was computed with the ORCA program<sup>25, 26</sup> at the PBE0 level using the 9s7p4d basis set on Co that was constructed specifically for EPR properties (full contraction scheme 621111111/3311111/3111),<sup>27</sup> and the IGLO-II basis<sup>28</sup> on the ligands (tight SCF convergence and fine integration grid, Grid5 option).

## References

1. K. Ackermann, A. Giannoulis, D. B. Cordes, A. M. Z. Slawin and B. E. Bode, *Chem. Commun.*, 2015, **51**, 5257-5260.
2. D. Akhmetzyanov, J. Plackmeyer, B. Endeward, V. Denysenkov and T. F. Prisner, *Phys. Chem. Chem. Phys.*, 2015, **17**, 6760-6766.
3. S. Milikisyants, F. Scarpelli, M. G. Finiguerra, M. Ubbink and M. Huber, *J. Magn. Reson.*, 2009, **201**, 48-56.
4. K. Keller, A. Doll, M. Qi, A. Godt, G. Jeschke and M. Yulikov, *J. Magn. Reson.*, 2016, **272**, 108-113.
5. R. G. Larsen and D. J. Singel, *J. Chem. Phys.*, 1993, **98**, 5134-5146.
6. A. D. Milov, K. M. Salikhov and M. D. Shirov, *Fiz. Tverd. Tela*, 1981, **23**, 975-982.
7. M. Pannier, S. Veit, A. Godt, G. Jeschke and H. W. Spiess, *J. Magn. Reson.*, 2000, **142**, 331-340.
8. P. A. S. Cruickshank, D. R. Bolton, D. A. Robertson, R. I. Hunter, R. J. Wylde and G. M. Smith, *Rev. Sci. Instrum.*, 2009, **80**, 1031021-10310214.
9. C. L. Motion, J. E. Lovett, S. Bell, S. L. Cassidy, P. A. S. Cruickshank, D. R. Bolton, R. I. Hunter, H. El Mkami, S. Van Doorslaer and G. M. Smith, *J. Phys. Chem. Lett.*, 2016, **7**, 1411-1415.
10. G. Jeschke, G. Panek, A. Godt, A. Bender and H. Paulsen, *Appl. Magn. Reson.*, 2004, **26**, 223-244.
11. G. Jeschke, V. Chechik, P. Ionita, A. Godt, H. Zimmermann, J. Banham, C. R. Timmel, D. Hilger and H. Jung, *Appl. Magn. Reson.*, 2006, **30**, 473-498.
12. Y. Polyhach, A. Godt, C. Bauer and G. Jeschke, *J. Magn. Reson.*, 2007, **185**, 118-129.
13. G. W. Reginsson, R. I. Hunter, P. A. S. Cruickshank, D. R. Bolton, S. T. Sigurdsson, G. M. Smith and O. Schiemann, *J. Magn. Reson.*, 2012, **216**, 175-182.
14. M. J. Frisch, G. W. Trucks, H. B. Schlegel, G. E. Scuseria, M. A. Robb, J. R. Cheeseman, G. Scalmani, V. Barone, B. Mennucci, G. A. Petersson, H. Nakatsuji, M. Caricato, X. Li, H. P. Hratchian, A. F. Izmaylov, J. Bloino, G. Zheng, J. L. Sonnenberg, M. Hada, M. Ehara, K. Toyota, R. Fukuda, J. Hasegawa, M. Ishida, T. Nakajima, Y. Honda, O. Kitao, H. Nakai, T. Vreven, J. J. A. Montgomery, J. E. Peralta, F. Ogliaro, M. Bearpark, J. J. Heyd, E. Brothers, K. N. Kudin, V. N. Staroverov, T. Keith, R. Kobayashi, J. Normand, K. Raghavachari, A. Rendell, J. C. Burant, S. S. Iyengar, J. Tomasi, M. Cossi, N. Rega, J. M. Millam, M. Klene, J. E. Knox, J. B. Cross, V. Bakken, C. Adamo, J. Jaramillo, R. Gomperts, R. E. Stratmann, O. Yazyev, A. J. Austin, R. Cammi, C. Pomelli, J. W. Ochterski, R. L. Martin, K. Morokuma, V. G. Zakrzewski, G. A. Voth, P. Salvador, J. J. Dannenberg, S. Dapprich, A. D. Daniels, O. Farkas, J. B. Foresman, J. V. Ortiz, J. Cioslowski and D. J. Fox, *Gaussian 09, Revision B.01*, Gaussian, Inc., 2010.
15. C. Adamo and V. Barone, *J. Chem. Phys.*, 1999, **110**, 6158-6170.
16. J. P. Perdew, in *Electronic Structure of Solids*, Ziesche, P.; Eischrig, H. Eds.: Akademie Verlag: Berlin, 1991.
17. J. P. Perdew, M. Emzerhof and K. Burke, *J. Chem. Phys.*, 1996, **105**, 9982-9985.

18. J. P. Perdew and Y. Wang, *Phys. Rev. B*, 1992, **45**, 13244-13249.
19. A. D. Becke and E. R. Johnson, *J. Chem. Phys.*, 2005, **122**, 154104-154101-154104-154102.
20. S. Grimme, J. Antony, S. Ehrlich and H. Krieg, *J. Chem. Phys.*, 2010, **132**, 154104-154101-1454104-1454119.
21. E. R. Johnson and A. D. Becke, *J. Chem. Phys.*, 2006, **124**, 174104-174101-174104-174109.
22. P. J. Hay, *J. Chem. Phys.*, 1977, **66**, 4377-4384.
23. A. J. Wacthers, *J. Chem. Phys.*, 1970, **52**, 1033-1036.
24. C. A. Kilner and M. A. Halcrow, *Dalton Trans.*, 2010, **39**, 9008-9012.
25. <https://orcaforum.cec.mpg.de> (accessed 01 August 2017).
26. F. Neese, *WIREs Comput. Mol. Sci.*, 2012, **2**, 73-78.
27. M. Munzarova and M. Kaupp, *J. Phys. Chem. A*, 1999, **103**, 9966-9983.
28. W. Kutzelnigg, U. Fleischer and S. M., in *NMR Basic Principles and Progress* ed. S.-V. Berlin, 1990, vol. 23, p. 165.